

**Key words:** *tip vortex, blade-vortex interaction*

ANDRZEJ SZUMOWSKI<sup>\*)</sup>, MIECZYŚLAW LITWIŃCZYK<sup>\*\*)</sup>

## ACTIVE CONTROL OF TIP VORTEX SHEDDING

A helicopter blade tip vortex generates impulsive noise of high intensity when it impinges upon the following blade. In the present work, the vortex is attenuated by coaxial swirling jet rotating in the opposite direction. The jet issues from a nozzle located at the blade tip. The nozzle was supplied with compressed air transported in the blade channel. The decrement of vortex strength is measured as a function of the compressed air pressure related to the dynamic pressure of the flow in the wind tunnel. It was found that the jet, even of relatively low intensity, considerably effects the blade tip vortex formation.

### 1. Introduction

For certain helicopter manoeuvres like descent with deep turns or low powered approach to landing, impulsive noise of high intensity is generated. This is due to the blade tip vortices impinging upon the following blades. In a general case, there are two possible ways to reduce the noise generated as a result of the blade vortex interaction (BVI): (i) by absorption of the acoustic energy (at least in part) directly in the region of interaction or (ii) by control of the tip vortex formation.

The acoustic energy can be absorbed by a porous material when it is used to cover the leading section of the blade [1]. The porosity, however, disturbs the boundary layer; it accelerates the laminar-turbulent transition and consequently increases the drag of the blade.

Therefore, the only practical way to diminish the BVI noise seems to be the control of the tip vortex shedding. Following this way, the previous investigators focused their attention on the blade tip shape considered as a control factor of the vortex formation. Various shapes of the blade tip shown in

---

<sup>\*)</sup> *Institute of Aeronautics and Applied Mechanics, Warsaw University of Technology; Nowowiejska 24, 00-665 Warsaw, Poland; E-mail: aszum@meil.pw.edu.pl*

<sup>\*\*\*)</sup> *Institute of Aeronautics and Applied Mechanics, Warsaw University of Technology; Nowowiejska 24, 00-665 Warsaw, Poland. E-mail: mlitw@meil.pw.edu.pl*

Fig. 1 were proposed [2], [3] to modify the shed vortex. Shapes “a” and “b” with a step change of chord length were predicted to generate two vortices of intensity lower than that of single vortex.

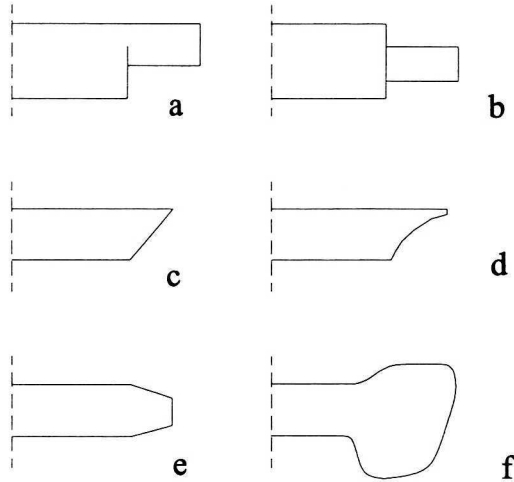


Fig. 1. Shapes of blade tips

To some extent, similar effects are achieved using the shapes “c”, “d” and “e”. In these cases, due to continuous changes of the chord length, the vorticity in the blade tip region is dispersed. In effect, the core of the shed vortex expands. Due to vortex dispersion, in each case of the blade tip presented above the tangential flow velocity induced by the vortex is diminished. As a result, the variations of the blade flow velocity and thereby the blade surface pressure are smaller when the vortex impinges on the blade or passes along it.

The rotor shown in Fig. 1f was designed to expand the retreating blade stall envelope without compromising high Mach number performance.

The radical way that can lead to weakening of the effect of the BVI phenomenon seems to be the reduction of the vorticity in the blade tip region. This can be achieved using the coaxial vortex rotating in the opposite direction to the tip vortex. Due to the interaction between vortices rotating in opposite directions, the tip vortex is expected to be suppressed or at least weakened. The swirling jet generator shown in Fig. 2 is based on this idea. It consists of a nozzle located at the blade tip, having a tangential inlet and an axial outlet. The nozzle is supplied with air transported in a channel inside the blade. The swirling jet from the nozzle issues into the centre of the tip vortex and in this way decreases its intensity. The air used to generate the swirling jet is additionally compressed by centrifugal forces existing due to rotation of the blade (see Appendix). The flow rate of the air can be controlled from the helicopter cockpit. It can be used only during the helicopter manoeuvres,

mentioned above, for which the BVI is significant as a noise generator. During the remaining phases of the helicopter flight the blade channel can be closed.

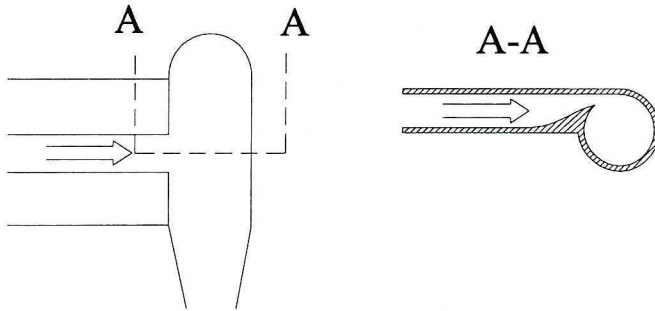


Fig. 2. Generator of swirling jet

This paper presents the experimental results of the tip vortex reduction due to a counter-rotating vortex.

## 1. Experimental set-up

Investigations were conducted in a wind tunnel with an opened test section of diameter 1.16 m. The blade with a profile (chord length  $c = 200$  mm) developed in the Institute of Aviation in Warsaw was used in the experiments. The blade tip was located in the centre of test section of the tunnel. A nozzle generating the swirling jet (Fig. 3) was mounted at the blade tip. It was supplied with compressed air transported through the blade channel from an external compressor.

The tip vortex line downstream of the blade was identified by means of a small tuft. The decrement of the vortex strength along this line was measured by means of a probe prepared in the present work. It contains a plate of dimensions  $50 \times 15 \times 0.2$  mm, parallel to the main flow direction in the test section, fixed to the axis of miniature electric generator. The voltage of the generator ( $U$ ) is proportional to the rotation velocity of the plate (driven by the vortex) and approximately proportional to the strength of the vortex.

The experiments were conducted for constant dynamic pressure of the flow in the test section  $q = 100$  Pa and two values of the angle of attack of the blade,  $\alpha = 4^\circ$  and  $8^\circ$ . The overpressure ( $p_0$ ) of the compressed air supplying the system was measured by means of a Pitot tube located at the inlet to the nozzle, and could be changed in the range from 0 to 3200 Pa.

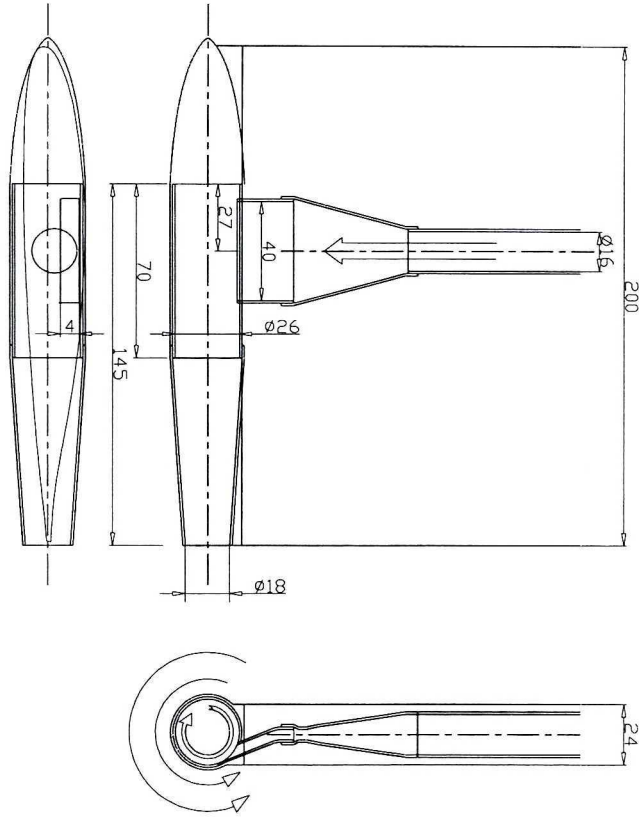


Fig. 3. Blade tip with swirl generator. Dimensions in mm

### 3. Results

The coordinate system shown in Fig. 4 was used to show the vortex line position. Coordinate  $x$  of this system is directed along the axis of the test section. Figures 5 and 6 present the location of the vortex lines for several values of the stagnation pressure of the compressed air ( $p_0$ ) normalised with the dynamic pressure of the flow in the test section ( $q$ ).

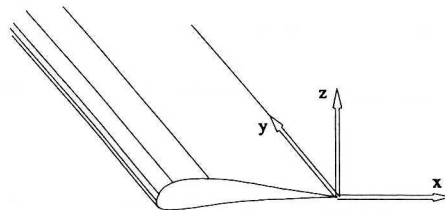


Fig. 4. Coordinate system

Two vortices: the main tip vortex and the secondary vortex of low intensity were noted (The latter exists for relatively high ratios  $S = p_0/q$  only). The positions of the vortices are marked in Figs 5 and 6 by empty and filled symbols, respectively. It is observed that the vortex line in both the  $xy$  and  $yz$  plane only slightly depends on the intensity of the swirling jet from the nozzle.

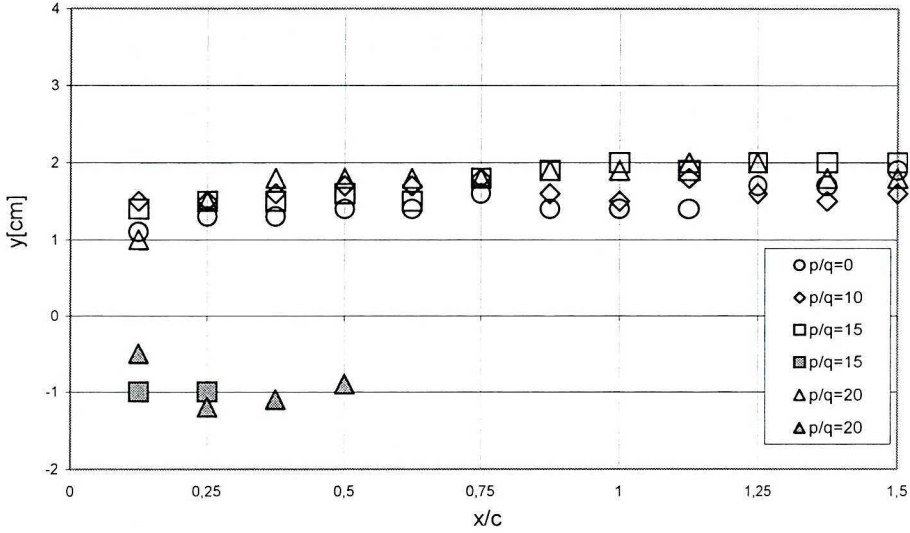


Fig. 5. Vortex centre positions in  $xy$  and  $xz$  planes,  $\alpha=4^\circ$

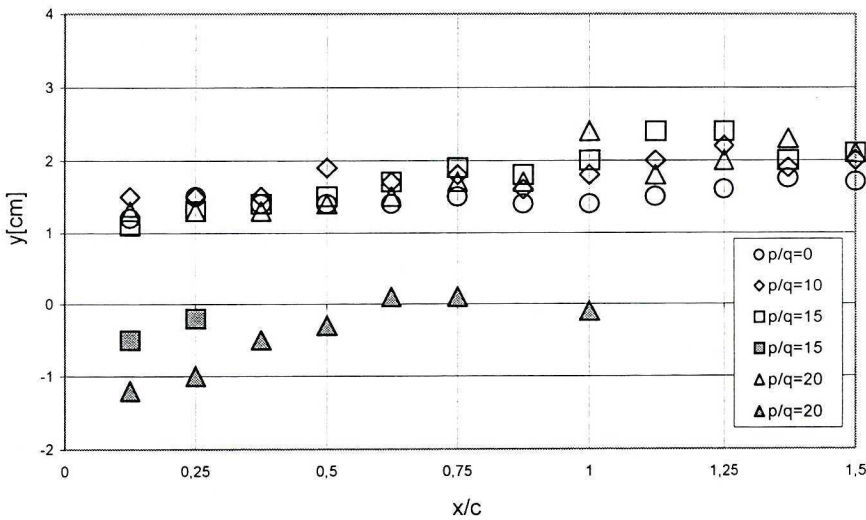
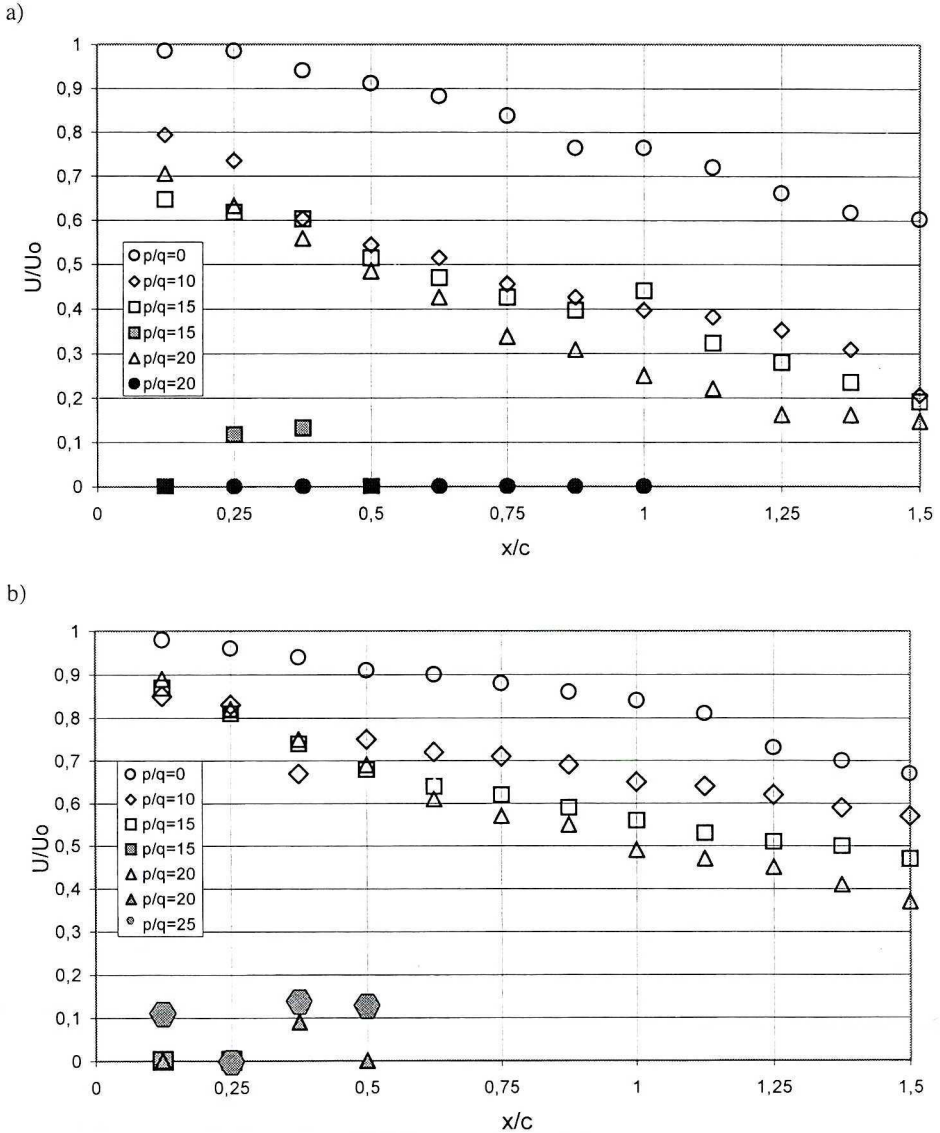


Fig. 6. Vortex centre positions in  $xy$  and  $xz$  planes,  $\alpha=8^\circ$

The variations of the relative vortex intensity, as it is carried away with the tunnel flow for several values of  $S$ , are presented in Fig. 7. The vortex intensity (voltage of the generator) at the trailing edge of the airfoil ( $x = 0$ ) was used to normalise all values.

One can note that the intensity of the vortex decreases along its line regardless of whether the vortex strength is reduced due to the swirling jet or not. However, the decrement of vortex intensity is larger when the swirling jet of opposite rotation is introduced.



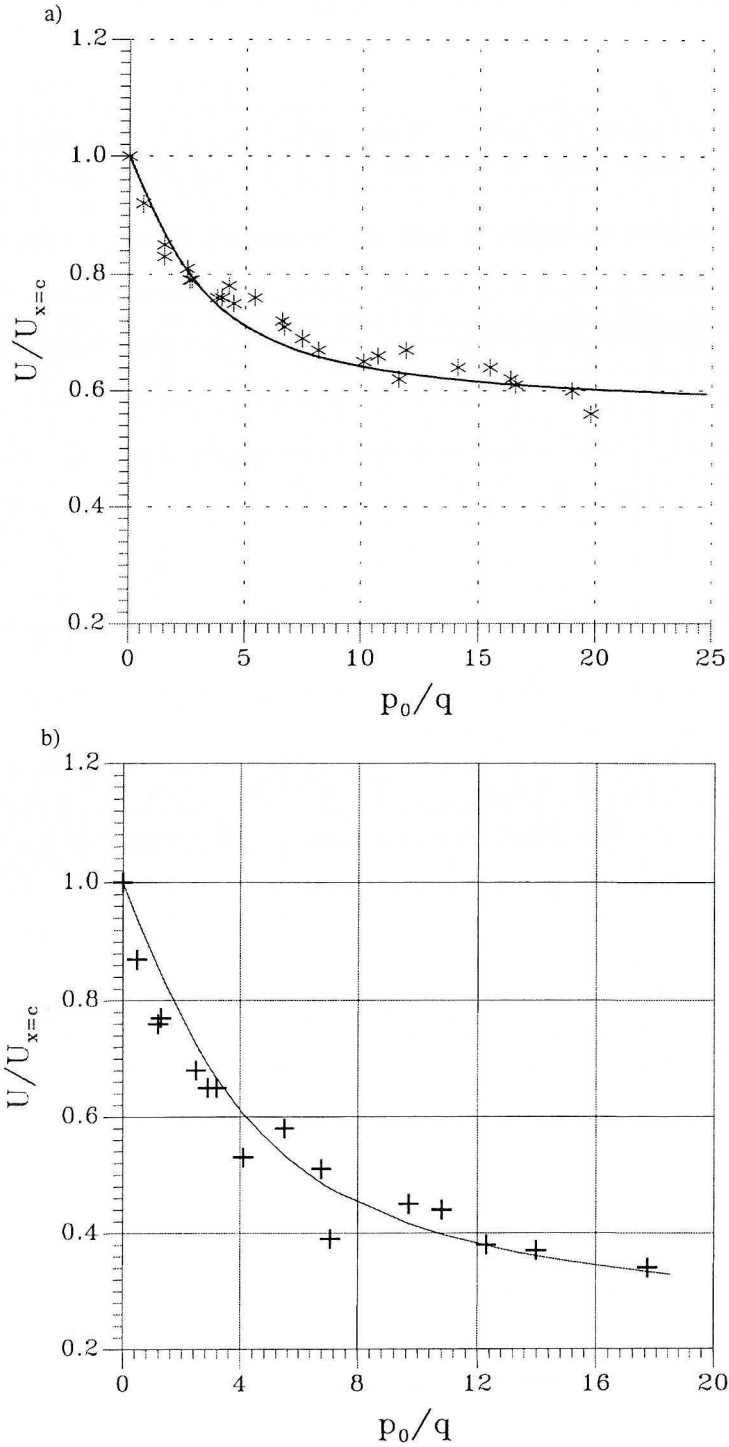


Fig. 8. Relative vortex intensity as a function of compressed air pressure,  $\alpha=8^\circ$  (a) and  $4^\circ$  (b); experimental points and curve fit

The effect of swirling jet on the tip vortex suppression is displayed in Fig. 8. The figure shows the relative vortex intensity measured a chord length downstream of the trailing edge of the blade. The intensity of natural tip vortex (without the swirling jet) at  $x/c=1$  is used to normalise the remaining cases. One can note that the tip vortex intensity distinctly decreases with the strength of swirling jet introduced into the vortex core. The decrement of vortex intensity is much higher for weak swirling jets (low  $p_o$ ) than for strong ones. It means that even a weak swirling jet could substantially weaken the tip vortex.

#### 4. Conclusions

The blade tip vortex can be effectively attenuated by a counter rotating coaxial swirling jet. This can be achieved for the jet even of relatively low intensity. The attenuation of the tip vortex takes place due to the suppression by the angular momentum of rotating jet and due to the increase of pressure in the vortex core. The latter effect leads to an increase of vortex core radius and, in consequence, to a decrease of induced tangential velocity. The air supplying the swirl generator, transported in the channel inside the blade, is additionally compressed due to centrifugal forces.

\*\*\*

### APPENDIX

#### Pipe flow supported by centrifugal forces

A channel inside the structure of the blade can be used to transport the air from a compressor to the vortex generator. The flow in the channel for a given supplied pressure is controlled by viscosity and centrifugal forces existing due to the rotation of the blade. Considering these effects, the flow can be described by the following governing equations. (For relative length of the channel  $l/D \cong \sim 200$  the one-dimensional model of the channel flow is assumed).

1. The continuity equation

$$\rho u = \text{const} \quad (1)$$

(for notation see at the end of the appendix).

2. The momentum equation of radial motion

$$u \frac{du}{dx} + \frac{1}{\rho} \frac{dp}{dr} = \omega^2 r - \frac{\lambda}{D} \frac{u^2}{2}. \quad (2)$$

3. The momentum equation of tangential motion

$$-\rho uv r + \left[ \rho uv + \frac{d}{dr} (\rho uv) dr \right] (r + dr) = dN,$$

which for  $\rho u = \text{const}$  and  $v = \omega r$  can be simplified to the following form

$$2\rho u\omega r dr = dN, \quad (3)$$

4. The energy equation for adiabatic flow

$$\frac{d}{dr} \left[ \rho u \left( h + \frac{u^2 + v^2}{2} \right) \right] dr = \omega dN. \quad (4)$$

The above equations can be supplemented with the equation of state  $p = \rho RT$  and the relationships based on the definition of enthalpy  $h = a^2/(k-1)$ , the flow Mach number  $M = u/a$ , the stagnation pressure  $p_0 = p \left[ 1 + 0.5(k-1)M^2 \right]^{k/(k-1)}$  and the stagnation speed of sound  $a_0^2 = a^2 \left[ 1 + 0.5(k-1)M^2 \right]$ .

Equations (1)-(4) and the supplemented relationships lead to the following differential equations for the flow Mach number and the pressure

$$\frac{dM^2}{d\bar{r}} = M^2 \frac{1 + 0.5(k-1)M^2}{1 - M^2} \left[ kM^2 \lambda \frac{l}{D} - (k+1) \frac{\bar{\omega}^2 \bar{r}}{\bar{a}_0^2} \right], \quad (5)$$

$$\frac{d\bar{p}}{d\bar{r}} = \frac{\bar{p}}{1 - M^2} \left\{ -\frac{kM^2}{2} \left[ 1 + (k-1)M^2 \right] \lambda \frac{l}{D} + k \left( 1 + \frac{k-1}{2} M^2 \right) \frac{\bar{\omega}^2 \bar{r}}{\bar{a}_0^2} \right\}, \quad (6)$$

where bars mean dimensionless values

$$\bar{r} = r/l,$$

$$\bar{\omega} = \omega l/a_{01},$$

$$\bar{a}_0 = a_0/a_{01} = 1 + 0.5(k-1)\bar{\omega}^2 \bar{r}^2,$$

$$\bar{p} = p/p_{01}.$$

The dimensionless stagnation pressure is

$$\bar{p}_0 = \bar{p}_0 / \bar{p}_{01} = \bar{p} \left( 1 + \frac{k-1}{2} M^2 \right)^{k/(k-1)}.$$

Figures 9a and 9b show the flow Mach number and stagnation pressure distributions obtained from Eqs.(5) and (6), respectively. The equations were solved for several values of  $M_1$  and  $p_0/p_a = 1$  both at  $x = 0$ . The flow Mach number  $M_1$  is proportional to the flow rate in the channel

$$Q = \frac{\pi D^2}{4} p_{01} \sqrt{\frac{k}{RT_o}} M \left( 1 + \frac{k-1}{2} M_1^2 \right)^{\frac{k+1}{2(k-1)}}.$$

One can note that the increase of the stagnation pressure  $(p_0)_{x=l} - (p_0)_{x=0} > 0$  for the data assumed in the present calculations exists for  $M_1 < \sim 0.3$ .

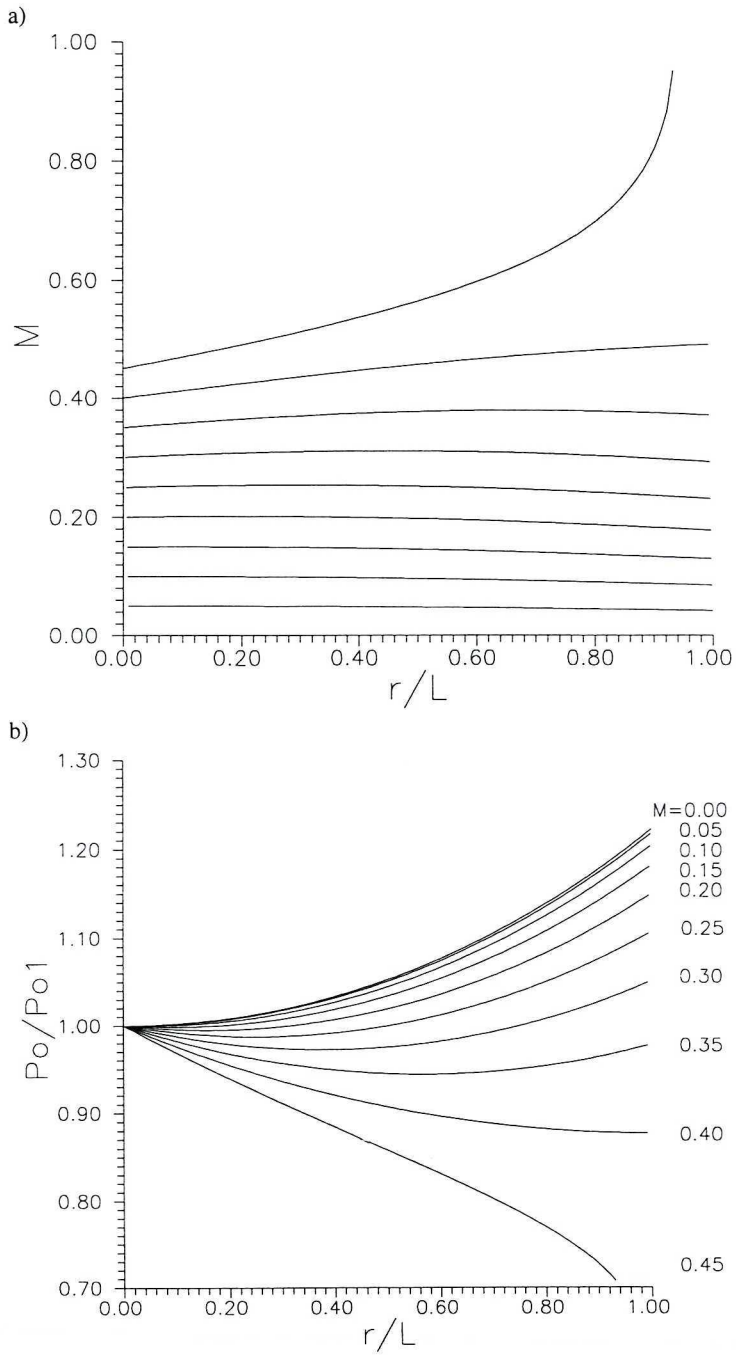


Fig. 9. Flow Mach number (a) and stagnation pressure (b) distributions along the blade.  
 $\lambda=0.01$ ,  $l=3.7\text{m}$ ,  $D=16\text{ mm}$ ,  $\bar{\omega} = 0.544$

## Nomenclature

$a$	speed of sound,
$a_0$	stagnation speed of sound,
$c$	chord length,
$D$	diameter of the channel cross-section,
$h$	enthalpy,
$k$	isentropic exponent,
$l$	length of the blade,
$M$	Mach number,
$N$	momentum of wall pressure of the channel,
$p$	pressure,
$p_0$	stagnation pressure,
$Q$	flow rate,
$r$	radius,
$u$	flow velocity in the blade channel,
$v$	tangential velocity of the blade,
$\omega$	speed of rotation,
$\lambda$	hydraulic coefficient,
$\rho$	density.

Index 1 corresponds to the conditions at  $r = 0$ .

Manuscript received by Editorial Board, March 01, 2001;  
final version, April 25, 2001.

## REFERENCES

- [1] Lee S.: Reduction of blade – vortex interaction noise through porous leading edge. AIAA Journal, vol.32, No. 3, 1994.
- [2] Montay W.R., Shindler P.A., Campbell R.T.: Some Results of the Testing of a Full-Scale Ogee-Tip Rotor. Journal of Aircraft, Vol.16, No 3, 1979.
- [3] Proceedings of the International Technical Meeting on Rotorcraft Acoustics and Rotor Fluid Dynamics. Philadelphia, Oct. 1991.

## Aktywne oddziaływanie na wir krawędziowy

### Streszczenie

Wir krawędziowy sphywający z końcówki łopaty helikoptera w pewnych fazach jego lotu oddziaływuje z kolejną łopatą. W wyniku generowany jest intensywny hałas o charakterze impulsowym. W pracy, do tłumienia wiru zastosowano współosiowy strumień zawirowany o przeciwnym niż wir kierunku rotacji. Strumień wytwarzany jest w dyszy umieszczonej na końcu łopaty zasilanej sprężonym powietrzem przesyłanym kanałem we wnętrzu dźwigara łopaty.

W wyniku badań wyznaczono zależność względnego natężenia wiru mierzonego w odległości jednej cięciwy od krawędzi opływu, w funkcji stosunku ciśnienia zasilania dyszy do ciśnienia dynamicznego w przestrzeni pomiarowej tunelu aerodynamicznego. Stwierdzono, że nawet względnie słaby strumień zawirowany wdmuchiwany do rdzenia wiru krawędziowego powoduje istotne osłabienie tego wiru.